Published in Energy http://dx.doi.org/10.1016/j.energy.2017.03.104

Author's post-print Version

Local resolved investigation of hydrogen crossover in polymer electrolyte fuel cell

Jing Shan[a, b, c], Pawel Gazdzicki[c], Rui Lin[a, b,*], Mathias Schulze[c], K. Andreas Friedrich[c,d]

[a] Clean Energy Automotive Engineering Centre, Tongji University, Shanghai 201804, Shanghai, China

[b] School of Automotive Studies, Tongji University, Shanghai 201804, Shanghai, China

[c] German Aerospace Center (DLR), Institute of Engineering Thermodynamics, Pfaffenwaldring 38-40, 70569 Stuttgart, Germany

[d] University of Stuttgart, Institute of Energy Storage, Pfaffenwaldring 31, 70569 Stuttgart, Germany

Abstract

In this study, the effects of temperature, pressure and relative humidity (RH) on hydrogen crossover rate from anode to cathode of a PEMFC is investigated. Segmented cells are used to measure the local hydrogen crossover current density (j_{H2}^{cross}) distribution. The results present approximate linear increase of the hydrogen crossover rate with increasing temperature and hydrogen back pressure with rates of 0.038 mA cm^{-2} K^{-1} and 3.33 mA cm^{-2} bar^{-1}, respectively. Generally, slightly increased H_2 crossover is observed in gas inlet areas than cell average. Unlike the approximate linear relationship between temperature or pressure with hydrogen crossover, the effect of relative humidification on hydrogen crossover is more complex with different increasing rate before fully humidification and dramatic decline at excessive humidification. It is demonstrated that segmented cells can be advantageously applied to study local H_2 crossover of intact MEAs.

Keywords hydrogen crossover; segmented cell; operating condition; PEMFC

1 Introduction

Proton Exchange Membrane Fuel Cells (PEMFC) have received considerable attention from researchers in the recent decades as a source of clean energy and as an alternative to conventional internal-combustion engines in automobile and transportation applications due to its high power density, high efficiency, zero emissions, nonmoving parts and silent operation. The main advantage of PEMFC arises from the emission free electricity generation by reacting oxygen and hydrogen to produce water and heat as the only byproducts.[1-3] However, PEMFC still faces several difficulties, such as high cost due to use of expensive materials and limited durability related to component degradation during operation [4]. Thus, a lot of emphasis has been given to study, understand, and alleviate these issues [5-7].

The polymer ion conducting membrane is a key component of membrane electrode assembly (MEA) of a PEMFC. In recent years thinner membranes have been developed to increase ionic conductivity and, hence, to increase the cell performance. However, with decreased membrane thickness other problems have arisen, such as reactant crossover (especially at low current densities) and reduced mechanical stability of the membrane.

Hydrogen crossover is the diffusion of hydrogen from the anode to the cathode through the membrane which occurs faster than the diffusion of other gases. Several groups [8-11] have investigated the effect of hydrogen crossover. Hydrogen crossover has at least three negative effects on fuel cell operation: fuel efficiency reduction, cathode potential depression, and aggressive peroxide radical formation [12]. Specifically, the hydrogen which crosses over can directly react with oxygen at the cathode surface, resulting in reduced cell voltage due to development of so called

mixed cathode potentials [13, 14]. H_2 and O_2 could also react directly at the cathode producing peroxide radicals at the same time, which not only attack the catalyst layer but also the membrane, causing significant catalyst layer and membrane degradation [15]. Wang et al. [16] demonstrated via ex-situ NMR (nuclear magnetic resonance) and FTIR (Fourier transform infrared spectroscopic) analysis of Nafion® based MEAs that the membrane degradation was originated from the decomposition of polymer main chain. It is speculated that with the increased loss of membrane units, small bubbles with the diameter of several microns started to form inside the membrane itself. These bubbles made the membrane vulnerable to hazards of gas crossover, which further led to a catastrophic failure of the proton exchange membrane. There are mainly two ways to form hydrogen peroxide, one being oxygen reduction at the cathode, the other based on the crossover of oxygen from the cathode to the anode. The hydrogen peroxide diffuses into the membrane and reacts with metal ions, present as impurities in the membrane to form HO• or HOO•, which can attack the polymer and degrade the membrane [17, 18]. In addition, hydrogen radical species have also been reported can degrade the membrane [19]. Therefore, the measurement of hydrogen crossover is of great importance for the fundamental understanding and practical mitigation of fuel cell degradation and membrane failure.

Effects of operating conditions on the hydrogen crossover has been investigated by several groups [15, 20, 21] but the detailed mechanism and locally evolving process of hydrogen crossover during the changing of operating conditions have not been clarified. In this study, we applied segmented cell measurements, which are powerful tools for in-operando monitoring of current density distribution [22-26], for locally resolved monitoring of the hydrogen crossover current density distribution. Segmented cells have been already demonstrated to be suitable to detect large

amounts of hydrogen crossover due to pinholes in the membrane [24]. To the best of our knowledge, however, they have not yet been used to investigate effects of cell temperature, back pressure and relative humidification on local hydrogen crossover distribution in intact MEAs.

2 Experimental

In this section, the test objects and segmented cell technology are firstly described. Afterwards the electrochemical method of measuring hydrogen crossover and methods of measuring the effects of temperature, back pressure and relative humidity on hydrogen crossover are described separately.

2.1 Test objects

Two different membrane electrode assemblies (MEAs) were used as test objects. MEA1 is a commercially available MEA from Wuhan Xinyuan Corporation with a perfluorosulfonic acid (PFSA) membrane with a thickness of 25 μm. The active electrode area was 50 cm^2. Single channel serpentine flow fields were applied on both electrodes of the cell. In order to keep the MEA, the gaskets and the segmented board in good contact, clamping pressure of 8 bars was provided by cylinder compression. Relative humidity was controlled by passing reactants through bubbler humidifiers. MEA2 is a commercially available product from Johnson Matthey Fuel Cells. The membrane thickness was 20 - 25 μm and the active electrode area was 25 cm^2. The experiments were conducted on a homemade single cell test bench at DLR (see affiliation above) in Stuttgart, Germany, using single channel serpentine flow fields. 50 cm^2 and 25 cm^2 cell plates are used for MEA1 and MEA2, respectively. The test

samples were conditioned at 1000 mA cm^{-2} with fully humidified gases for 20 hours. Stoichiometry ratios were 1.5 and 2.0 for hydrogen and air, respectively.

2.2 Segmented cell technology

To investigate the locally resolved hydrogen crossover current density, the segmented printed circuit broad (PCB) technology [22 - 24, 27] was adopted. The segmented flow field plate integrated with temperature sensors was installed between the MEA and the anode current collector plate. Our previous study [24] ascertained the assumption of identical current density distributions in anode and cathode by integrating segmented bipolar plates on both sides of the cell. The identical current density distributions obtained indicate negligible lateral currents due to high conductivity perpendicular to the membrane plane compared to the in-plane conductivity and the anode and cathode current density distributions are equivalent. The current density distribution data were collected using a data acquisition unit consisting of a multiplexer and a digital multimeter. In this study, two segmented plates with the same segment configuration but different segment size were used for MEA1 and MEA2, respectively.

2.3 Measuring hydrogen crossover rate

After the conditioning procedure a nitrogen flow was introduced into the cathode to remove the air and the anodic H_2 flow was set at a constant rate. The specific flow of nitrogen was 120 ml min^{-1} for MEA1 and 60 ml min^{-1} for MEA2. The hydrogen flow was 380 ml min^{-1} for MEA1 and 190 ml min^{-1} for MEA2. After 20 mins of N_2 flushing, the cathode potential was below 120 mV. Then a Zahner IM6 potentiostat was connected to the fuel cell for H_2 crossover measurements, with the working electrode probe connected to the cathode and the counter/reference electrode probes

connected together to the anode. The current produced from the oxidation of crossed H_2 from the anode was measured at a potential of 0.4 V. At this cathode potential, all H_2 that has crossed over from the anode to the cathode should be completely oxidized, producing a current (J_{H2}^{cross}) indicating the amount of hydrogen that has crossed over. The molar permeation flux density (φ) of hydrogen through the membrane is determined by the measured crossover current densities (j_{H2}^{cross}) using Faraday's law

$$\varphi = \frac{j_{H2}^{cross}}{zF} \quad (1)$$

Throughout the whole experiment the hydrogen crossover current density distribution was recorded using a segmented plate.

2.4 Effects of temperature and back pressure on H_2 crossover rate

MEA1 was used in this section. Throughout the experiment the RH was kept at 100% for both electrodes. The investigated cell temperature range was from 50 °C to 80 °C and the investigated back pressure range was from 1.4 bars to 1.9 bars absolute pressure. Throughout the experiment, j_{H2}^{cross} was recorded by a 50 cm^2 segmented plate.

2.5 Effects of relative humidity on H_2 crossover rate

To analyze the effect of relative humidity on hydrogen crossover MEA2 was used. The RH range, controlled by adjusting the dew point temperature of bubbler humidifiers, was from 50% to excessive humidification. Back pressures were kept at 1.5 absolute bars for both electrodes and cell temperature was kept constant at 80 °C. j_{H2}^{cross} distribution was recorded throughout the experiment using a 25 cm^2 segmented plate.

3 Results and discussion

3.1 Effects of cell temperature on H_2 crossover

Fig. 1 shows the H_2 crossover current density j_{H2}^{cross} in cell temperature range of 50 °C to 80 °C at 100% relative humidity. In the individual panels j_{H2}^{cross} is plotted as an average value of the entire cell (A), gas inlet area (B), center flow field area (C), and gas outlet area (D). The data is determined from segmented cell measurements depicted in Figure 2. In accordance with Inaba et al. [28] it was found that the average hydrogen crossover current density increases with temperature. In panel (A) an almost linearly dependence of j_{H2}^{cross} on T_{cell} is observed with a slope of 0.038 mA cm^{-2} K^{-1}. From a thermodynamic perspective, gas diffusion through polymers is due to random thermal movement of gas molecules in the polymer structure as reviewed by Rogers [29]. Through thermally activated jumps, gas molecules can permeate across the barriers comprised of van der Waals force between the polymer chains [30]. So when temperature increases, the thermally activated hydrogen molecules could permeate across more barriers which lead to an increased hydrogen diffusion coefficient. From the perspective of microscopic structure of the membrane, the flexibility of the membrane increases with increasing temperature [28, 31]. Apart from that, the movement of the hydrophobic backbone in the PFSA membrane is facilitated at elevated temperatures, resulting in increased free volume for the hydrogen crossover in the PFSA membrane [32].

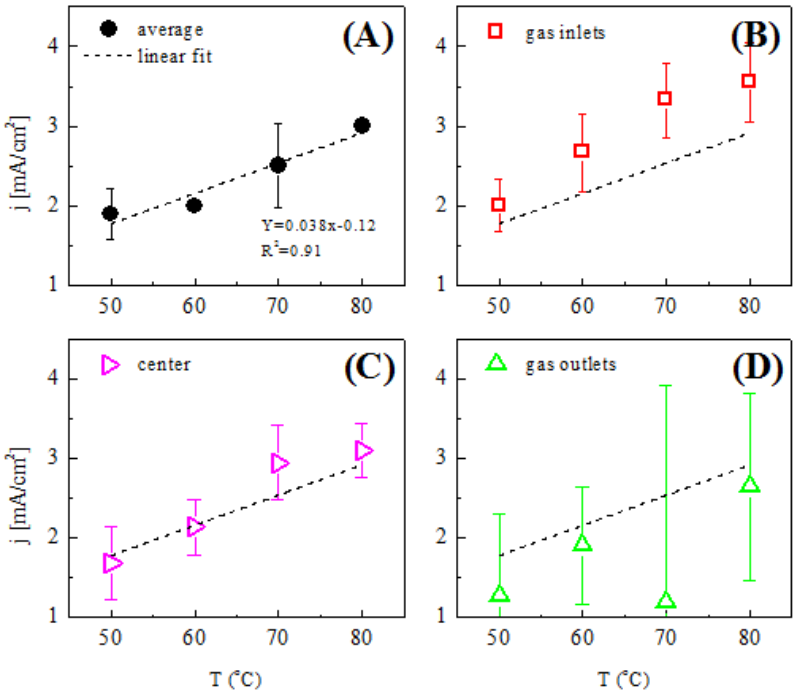

Fig. 1 H_2 crossover current density at different cell temperature of MEA1. (H_2 flow: 380 ml min^{-1}, N_2 flow: 120 ml min^{-1}, 100% RH, back pressure: 1.5 bars absolute pressure for both electrodes). In (A) the average current density of the entire cell is plotted along with a linear fit (included in other panels for comparison). In (B) the gas inlet area corresponds to segments in lines 1 and 2 according to the images in Figure 2. Center area is defined as segments of lines 3, 4, and 5 (C). Gas outlet area corresponds to segments of lines 6 and 7.

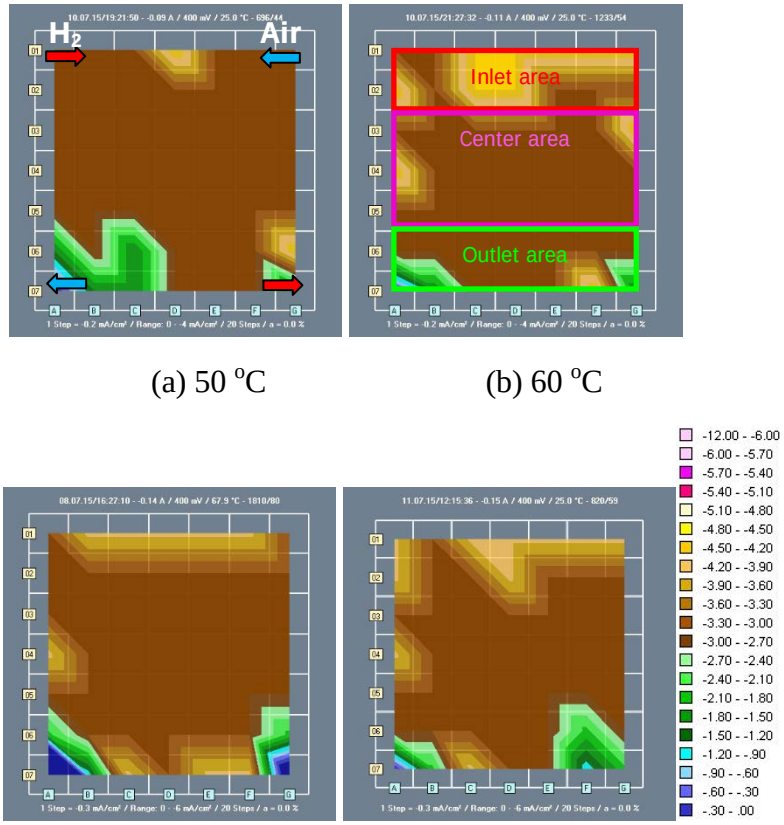

(a) 50 °C (b) 60 °C

(c) 70 °C (d) 80 °C

Fig. 2 The evolution of j_{H2}^{cross} distributions (mA cm^{-2}) of MEA1 fed with fully humidified H_2/N_2 (H_2:380 ml min^{-1}, N_2: 120 ml min^{-1}) with the increase of cell temperature at 100% RH for both electrodes. In (b) the definition of the different flow field areas is illustrated. (Segment A1 and G7 are inlet and outlet of hydrogen. G1 and A7 are inlet and outlet of air.)

In Fig. 1 and Fig. 2, it can be observed that j_{H2}^{cross} is the highest at the gas inlet area. The values at the center area correspond to the cell average current density which is in the same range as observed by Inaba et al. [28]. The relatively low H_2 crossover at the outlets with very high fluctuations is likely due to periodic accumulation and blowing out of condensed water. Moreover, it could also be observed in Fig. 2 that segment A7 and G7, which correspond to outlet of air and hydrogen, indicate distinct low hydrogen crossover. This is caused by relative low temperature of outlets and blocking of hydrogen permeating pathway by condensed water. Generally, with

increasing cell temperature the crossover rate increases but the H_2 crossover distribution remains largely unchanged.

3.2 Effects of back pressure on H_2 crossover

The main permeating path of hydrogen molecules is the aqueous phase that constructs the proton conducting water channels [33]. The pressures applied in PEMFC are smaller than the capillary pressures in the water channels, which are estimated by Eikerling [34] to be in the order of 100 bars. Hence, the transport of gases through the water channels of Nafion is not driven by differential pressure but by diffusion.

A concentration difference Δc of molecules over a distance d, here d is the membrane thickness, yields a molar permeation flux density φ, as described by Fick's law [30]

$$\varphi = -D\frac{\Delta c}{d} \tag{3}$$

where D represents the diffusion coefficient of the gas in the considered medium. The permeated hydrogen molecules will be oxidized instantaneously as soon as it reaches the cathode catalyst layer at the applied voltage. So in our study, Δc is approximated to be the concentration in the anode side, eq (4) could be modified as

$$\varphi = -D\frac{c_{anode}}{d} \tag{4}$$

According to Henry's law, the H_2 concentration at anode is proportional to the pressure in our considered pressure range. So the c_{anode} here is approximated to be proportional to the anode hydrogen partial pressure P_{H2}

$$\varphi = -D\frac{P_{H2} * S}{d} \tag{5}$$

where S is the scale factor that is independent of the pressure in our considered pressure range. In our study, the feeding gas was 100% humidified at 80 ^{o}C before introducing into the anode so the total anode inlet pressure P_{inlet} (the inlet pressure was assumed to be equal to the back pressure) is the sum of hydrogen partial pressure and water vapor partial pressure P_{vapor}

$$P_{inlet} = P_{H2} + P_{vapor} \tag{6}$$

Combined eq (5) with eq (6), the following equations could be obtained

$$\varphi = -D\frac{\left(P_{inlet} - P_{vapor}\right) * S}{d} \tag{7}$$

$$\varphi = -\frac{DS}{d}P_{inlet} + \frac{DS}{d}P_{vapor} \tag{8}$$

With a constant P_{vapor} at 80 ^{o}C and $\frac{DS}{d}$ independent of pressure in our considered pressure range, the hydrogen permeating flux φ is approximately proportional to anode inlet pressure P_{inlet}.

The effects of anode back pressure on j_{H2}^{cross} is demonstrated in Fig. 3. By linear fitting, the average j_{H2}^{cross} of the entire cell in Fig. 3 (A) shows a goodness of fit R^2 = 0.96 and a slope of 3.331 mA cm^{-2} bar^{-1}. The measurement results confirmed our assumption of a close linear relationship between anode hydrogen partial pressure and hydrogen crossover rate. However, in literature a deviation from the linear behavior was observed when further decreasing the pressure down to ambient pressure [28]. According to Fig. 3 (B) and (C) that the j_{H2}^{cross} in gas inlet area is always above the average fit curve and the j_{H2}^{cross} in center area is above the average fit curve below 1.7 absolute bars and lower than average value when anode back pressure is higher than

1.7 absolute bars. This could also be observed in Fig. 4 which shows the local j_{H2}^{cross} distribution at different anode back pressures. Moreover, the j_{H2}^{cross} increasing rate in inlet and center area slows down starting from 1.7 absolute bars. The j_{H2}^{cross} in outlet area is always below the average fit curve but the increasing rate bounces back starting from 1.7 absolute bars. This could be attributed to the pressure loss along the flow field which means the local hydrogen pressure decreases from inlet area to outlet area. However the absolute pressure loss is almost constant in this pressure range which means the relative pressure loss decreases with increasing anode back pressure from inlet area to outlet area. So the j_{H2}^{cross} points approach average fit curve in outlet area at high back pressure level and the j_{H2}^{cross} homogeneity of the entire cell increases which could be indicated by the decreased standard deviation in Fig. 3(A). The abnormal value in Fig. 3(D) at 1.5 and 1.6 absolute bars could be caused by the flooding water which blocks the hydrogen permeating pathway.

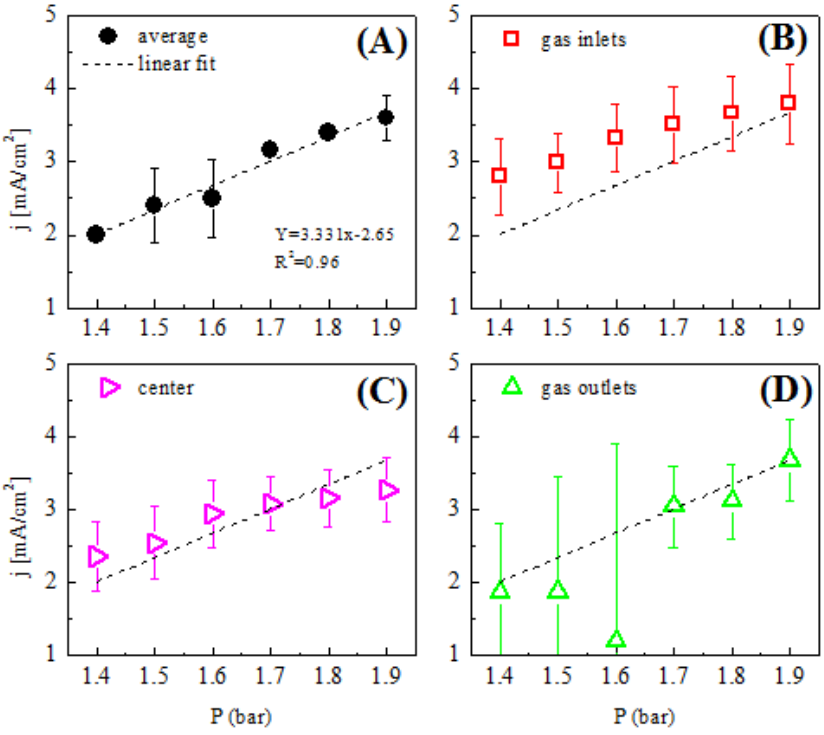

Fig. 3 H_2 crossover current density at different anode back pressures of MEA1. (H_2 flow: 380 ml min^{-1}, N_2 flow: 120 ml min^{-1}, 100% RH, T_{cell}=80 ^oC). In (A) the average current density of the entire cell is plotted along with a linear fit (included in other panels for comparison). In (B) the gas inlet area corresponds to segments in lines 1 and 2 according to the images in Figure 4. Center area is defined as segments of lines 3, 4, and 5 (C). Gas outlet area corresponds to segments of lines 6 and 7.

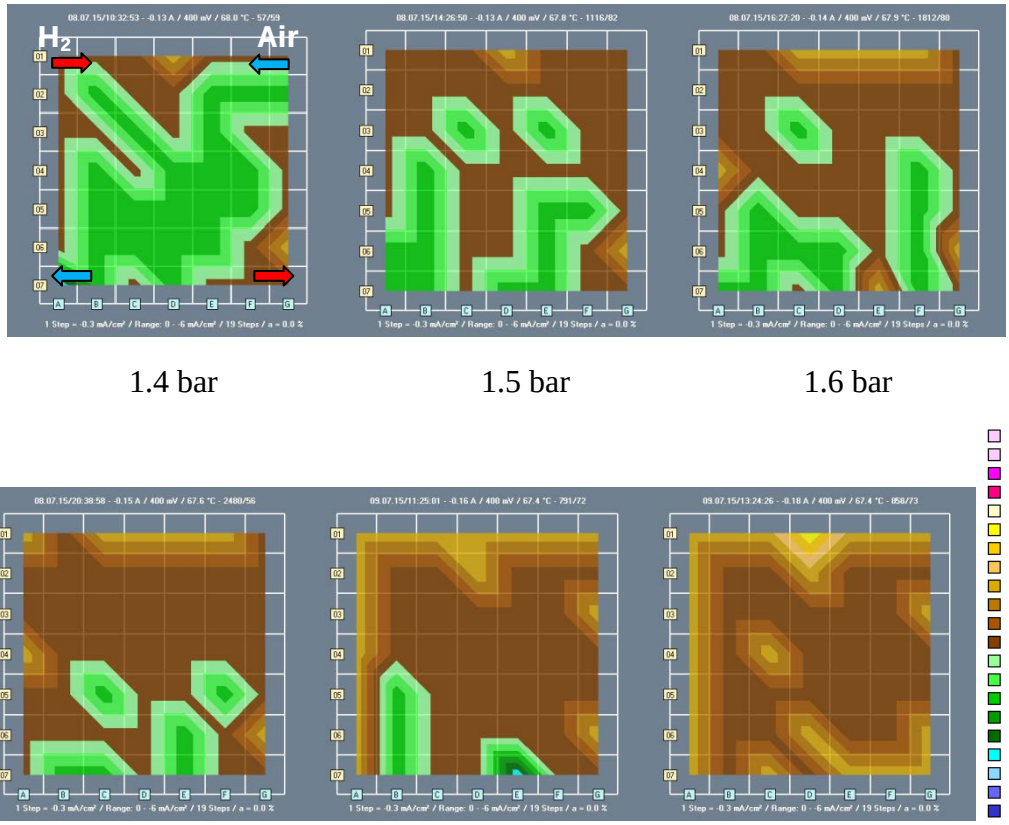

1.4 bar 1.5 bar 1.6 bar

1.7 bar 1.8 bar 1.9 bar

Fig. 4 The evolution of j_{H2}^{cross} distributions (mA cm^{-2}) of MEA1 fed with fully humidified H_2/N_2 (H_2:380 ml min^{-1}, N_2: 120 ml min^{-1}) with the increase of back pressure at both electrodes at steady state. (Segment A1 and G7 are inlet and outlet of hydrogen. G1 and A7 are inlet and outlet of air.)

In Fig. 4, the j_{H2}^{cross} in cathode outlet area is always the lowest of the entire cell. This is even more distinct in Fig. 5 which presents the j_{H2}^{cross} distribution at the initial stage (when voltage applied at cathode was 150 mV) of measurement procedure for the cell fed with H_2/N_2 at different back pressures. Permeated H_2 from anode to cathode would fully react with O_2 in air at general operating conditions or would be oxidized electrochemically by the hydrogen crossover measurement procedure. It can be observed in Fig. 5 that j_{H2}^{cross} is abnormally low at the outlet of cathode. N_2 was introduced to cathode for about 20 mins to remove air before the electrochemical measurement. Even though, there may still be some air left in the cathode catalyst layer especially the cathode outlet area where pressure of the purging nitrogen is

relative low due to pressure loss along the flow field. The crossed hydrogen will react with oxygen in remaining air directly without producing oxidation current. It can be observed in Fig. 5 that with increasing anode back pressure the phenomena became less distinct since higher purging pressure is favorable for the removal of remaining air in cathode catalyst layer. With the consumption of oxygen in remaining air and the rising of cathode potential the j_{H2}^{cross} at cathode outlet area gradually increases.

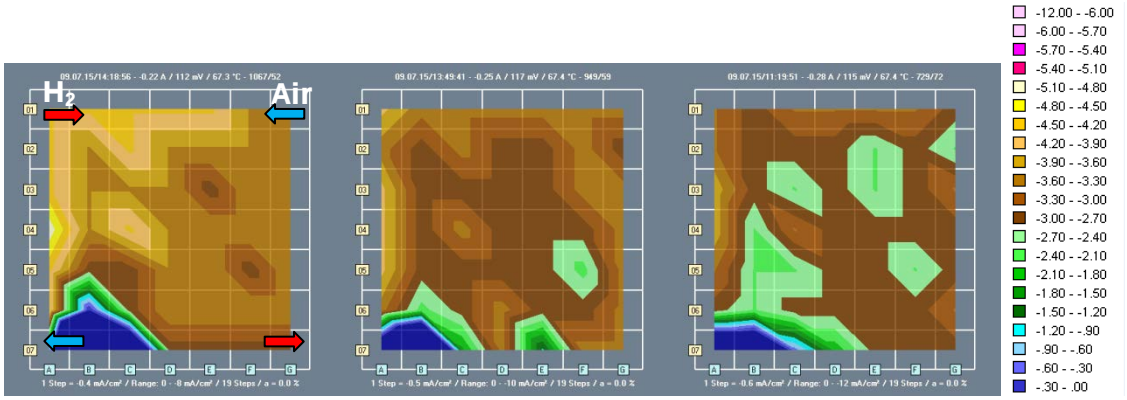

1.4bar 1.6 bar 1.8 bar

Fig. 5 The j_{H2}^{cross} distributions (mA cm^{-2}) at the initial stage (when voltage applied at cathode was 150 mV) of MEA1 fed with fully humidified H_2/N_2 (H_2:380 ml min^{-1}, N_2: 120 ml min^{-1}) at different back pressures. (Segment A1 and G7 are inlet and outlet of hydrogen. G1 and A7 are inlet and outlet of air.)

3.3 Effects of relative humidity on H_2 crossover

Fig. 6 shows the polarization curves of MEA2 at different humidification. It can be observed that the performance increased with RH increasing from 50% to 90%; above 90% no significant performance improvement was observed. Apart from that, no dramatic performance decline could be observed at high current density region which means little concentration loss at gas diffusion and catalyst layers. Furthermore, no flooding has occurred even at fully humidification condition in the studied current density range. The work by Bensmann [15] has reported that the influence of RH on hydrogen crossover is more complex than that of temperature and back pressure

where approximate linear dependencies are observed. According to Fig. 7(A) H_2 crossover current density increased non-linearly when RH was increased from 50% to 100% and then j_{H2}^{cross} decreased when RH exceeded 100%. The behavior for RH < 100% is consistent with the study by Inaba et al. [28] which covers the RH range 40 – 80%. For the sake of completeness it is noted that at dry conditions an increased H_2 crossover rate is observed due to reduced membrane tightness which becomes subsequently reduced with slightly increasing humidification [35]. In our experiment, starting at RH=50%, increasing RH will increase the water content in the membrane, which may increase both H_2 solubility and diffusion coefficients thus increase H_2 crossover. However, based on eq (6), for a controlled anode inlet pressure and constant cell temperature, the increase in RH would lead to the increase of vapor partial pressure P_{vapor} and decrease of hydrogen partial pressure P_{H2}. As has been studied in 3.2, a reduced hydrogen partial pressure would lead to a reduced j_{H2}^{cross}. So from 50% to 100% RH the effect of increasing H_2 solubility and diffusion coefficient was bigger than that caused by P_{H2} reduction, resulting in increased hydrogen crossover. With the H_2 solubility and diffusion coefficient approaching saturation, the P_{H2} reduction began to slow the j_{H2}^{cross} increasing rate down when RH increased from 70% to 100%. j_{H2}^{cross} began to decline at excessive humidification most likely due to flooding of gas diffusion and catalyst layers which hinders hydrogen crossover.

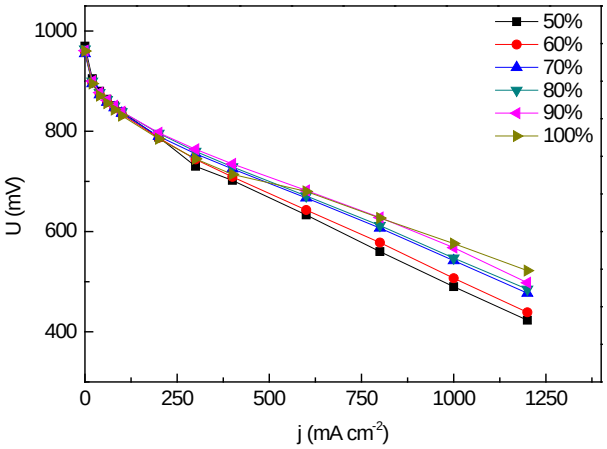

Fig. 6 Polarization curves of MEA2 at different humidification. (T_{cell}=80 ^{o}C, back pressure: 1.5 absolute bars for both electrodes, stoichiometry H_2/Air:1.5/2.0)

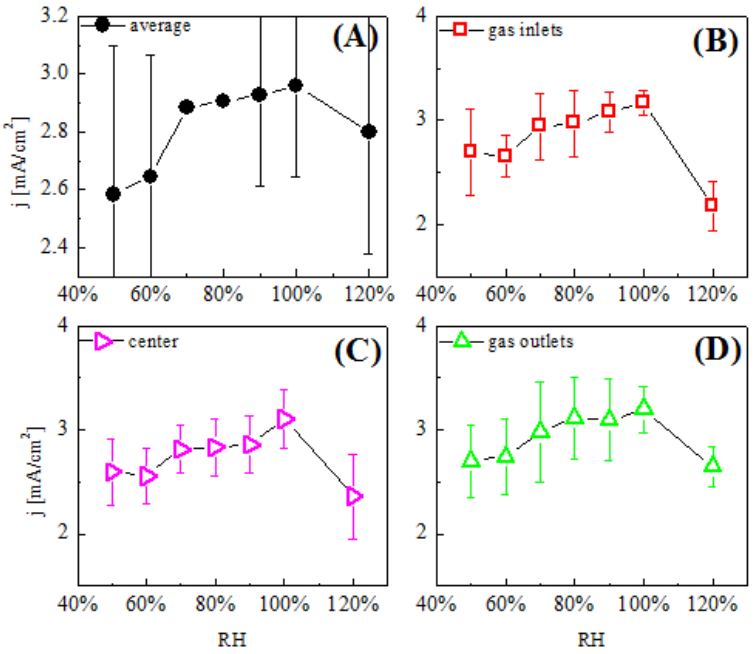

Fig. 7 The influence of relative humidity on hydrogen crossover of MEA2. (T_{cell}=80 ^{o}C, 1.5 bars absolute back pressure for both electrodes, H_2 flow: 60 ml min^{-1}, N_2 flow: 190 ml min^{-1}) In (A) the average current density of the entire cell is plotted along with a linear fit (included in other panels for comparison). In (B) the gas inlet area corresponds to segments in lines 1 and 2 according to the images in Figure 8. Center area is defined as segments of lines 3, 4, and 5 (C). Gas outlet area corresponds to segments of lines 6 and 7. Pay attention to different Y axis scale in (A).

Fig. 7(A) could also be explained from the perspective of membrane microscopic structure. The hydrated PFSA membrane is composed of three phases: a hydrophobic

phase formed by the fluorocarbon backbone chain, a hydrophilic phase by the ionic clusters of sulfonic ions and an intermediate phase formed by the side chain [32, 36]. The hydrophilic phase is responsible for the water uptake in PFSA membrane. Water uptake of the PFSA membrane at low RH results in the rearrangement of the hydrophobic backbone due to an elevated flexibility. Such rearrangement would create more free volume at the intermediate phase for hydrogen crossover. Free volume has the least resistance for hydrogen crossover so the crossover rate increased rapidly from 50% to 70% RH especially from 60% to 70% RH. Interestingly, the cell performance in Fig. 6 also shows significant improvement from 60% to 70% RH. This could be caused by the transition of proton conducting mechanism in the membrane from vehicle mechanism to hopping mechanism or Grotthuss mechanism [37] with increasing humidification. Further water uptake of the PFSA membrane would lead to the construction of water channels due to the combination of water molecules with ionic clusters in hydrophilic phase. The gas permeability of water channels is less than void volume but much higher than solid phase of PEM. So a slow hydrogen crossover increasing rate was observed from 70% to 100% RH in Fig. 7(A). Water uptake by Nafion membrane from liquid water (RH>100%) is higher than that from saturated water vapor [38]. This difference in water uptake can be explained by Schroeder's paradox [39]. Based on this paradox, the lower water uptake from vapor phase might be due to the hindered condensation of vapor within the pores of the membrane, which means at 100% RH there may still be some pores occupied by water vapor available for hydrogen permeation. Furthermore, it has been demonstrated that Nafion forms a skin layer of ca. 5 nanometers at the water vapor interface that represents a significant barrier to water uptake [40, 41]. This layer, however, undergoes reconstruction at the liquid water interface and water uptake is

improved. Hence, a decrease in hydrogen crossover was observed at excessive humidification [32]. Fig. 7(B), (C), (D) show similar evolving trend of hydrogen crossover with increasing RH which indicate largely homogeneous humidification state of the membrane. Fig. 8 shows the evolution of hydrogen crossover current density distribution of MEA2 at different humidification. A relative high hydrogen crossover could be observed in hydrogen outlet area. This could be attributed to the better humidification state of the membrane in this area. For 120% RH (dew point temperature of bubblers (84.5°C) higher than cell temperature (80°C)) a locally decreased hydrogen crossover in cathode inlet area is observed which is likely due to the blockage of hydrogen permeating pathway by condensed water at excessive humidification.

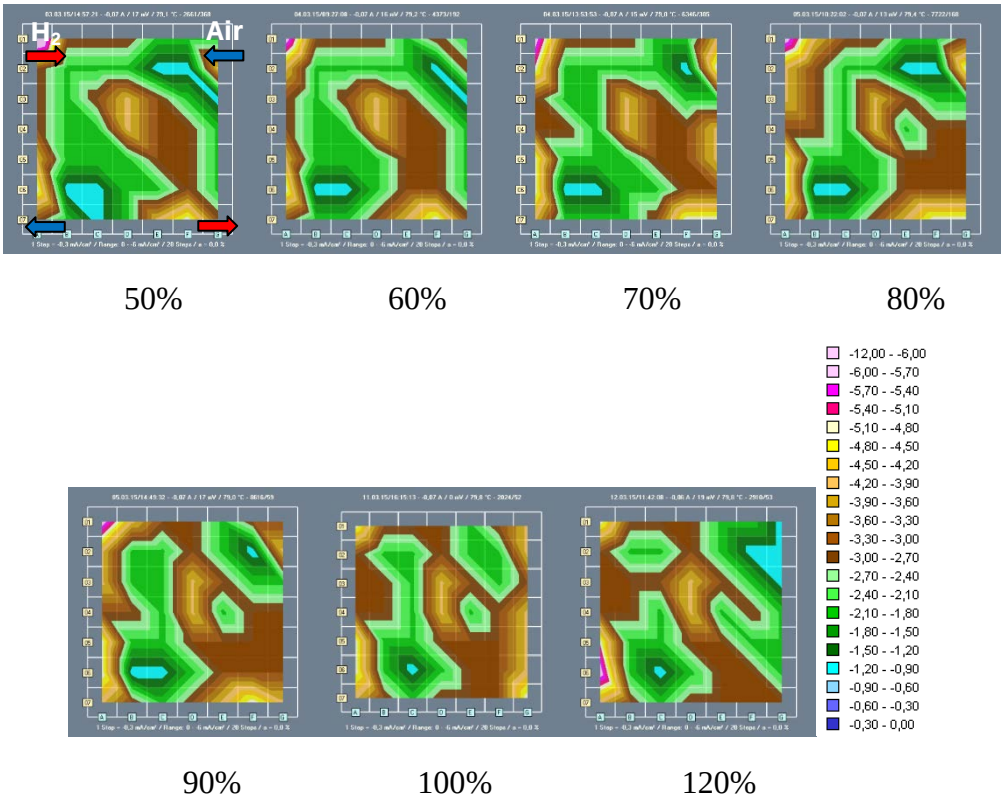

Fig. 8 The evolution of hydrogen crossover current density distribution of MEA2 at different reactant gases humidification. (T_{cell}=80 ^{o}C, 1.5 bars absolute back pressure for both electrodes, H_2 flow: 60 ml min^{-1}, N_2 flow: 190 ml min^{-1}, segment A1 and G7 are inlet and outlet of hydrogen. G1 and A7 are inlet and outlet of air.).

In previous studies [24] segmented cell measurements have been used to study H_2 crossover of defected MEAs in which a pinhole has emerged due to a sudden pressure drop of reactant gases. Bodner et al. used segmented cells to study the localization of artificial pinholes in MEAs [42]. In the case of membrane defects j_{H2}^{cross} reached values up to 300 mA cm^{-2} which are substantially higher than the crossover values of intact membranes shown in this paper. Therefore, our results show that local j_{H2}^{cross} distribution of different intact membranes can be positively analyzed using the segmented cell technology under different conditions.

4 Conclusions

In this study, the segmented cell technology was applied for the first time to study local H_2 crossover of intact MEAs versus cell temperature, gas pressure and humidity. From the measurements following conclusions have been drawn:

– A linear increase of H_2 crossover with increasing temperature and hydrogen back pressure was observed. Thereby, H_2 crossover was higher in the gas inlet area than cell average.

- RH has a smaller effect on H_2 crossover than that of temperature or pressure. The dependence of H_2 crossover rate is non-linear increasing for RH increasing up to 100 % and decreasing at excessive humidification: The measured H_2 current density distribution is homogeneous at all studied RH values.
- The effect of RH on H_2 crossover is explained by taking into account the H_2 partial pressure, H_2 solubility and diffusion coefficients in the membrane as well as microscopic structure of the membrane at different humidification levels.

Acknowledgements

This work was supported by the National Natural Science Foundation of China (No. 21276199), The Young Talents "Climbing" Program of Tongji University, The Fundamental Research Funds for the Central Universities and 111 Project (No. B08019).

The research leading to these results has received funding from the European Union's Seventh Framework Programme (FP7/2007-2013) for Fuel Cell and Hydrogen Joint Technology Initiative under Grant No. 303452 (Impact)

References

[1] L. Guétaz, S. Escribano, O. Sicardy, Journal of Power Sources, 212 (2012) 169-178.

[2] C. Bao, W.G. Bessler, Journal of Power Sources, 278 (2015) 675-682.

[3] R. Lin, B. Li, Y.P. Hou, J.M. Ma, International Journal of Hydrogen Energy, 34 (2009) 2369-2376.

[4] A. Alaswad, A. Baroutaji, H. Achour, J. Carton, A. Al Makky, A.G. Olabi, International Journal of Hydrogen Energy, 41 (2016) 16499-16508.

[5] S. Enz, T.A. Dao, M. Messerschmidt, J. Scholta, Journal of Power Sources, 274 (2015) 521-535.

[6] Y.-H. Lai, G.W. Fly, Journal of Power Sources, 274 (2015) 1162-1172.

[7] S. Zhang, X.-Z. Yuan, J.N.C. Hin, H. Wang, K.A. Friedrich, M. Schulze, Journal of Power Sources, 194 (2009) 588-600.

[8] R.N. Carter, S.S. Kocha, F. Wagner, M. Fay, H.A. Gasteiger, Ecs Transactions, 11 (2007).

[9] I.A. Schneider, D. Kramer, A. Wokaun, G.G. Scherer, Electrochemistry Communications, 9 (2007) 1607-1612.

[10] I.M. Kong, A. Jung, B.J. Kim, K.D. Baik, M.S. Kim, Energy, 93 (2015) 57-66.

[11] P. Sayadi, S. Rowshanzamir, M.J. Parnian, Energy, 94 (2016) 292-303.

[12] C. Francia, V.S. Ijeri, S. Specchia, P. Spinelli, Journal of Power Sources, 196 (2011) 1833-1839.

[13] S. Takaichi, H. Uchida, M. Watanabe, Electrochemistry Communications, 9 (2007) 1975-1979.

[14] J. Zhang, Y. Tang, C. Song, J. Zhang, H. Wang, Journal of Power Sources, 163 (2006) 532-537.

[15] B. Bensmann, R. Hanke-Rauschenbach, K. Sundmacher, International Journal of Hydrogen Energy, 39 (2014) 49-53.

[16] F. Wang, H. Tang, M. Pan, D. Li, International Journal of Hydrogen Energy, 33 (2008) 2283-2288.

[17] T. Kinumoto, M. Inaba, Y. Nakayama, K. Ogata, R. Umebayashi, A. Tasaka, Y. Iriyama, T. Abe, Z. Ogumi, Journal of Power Sources, 158 (2006) 1222-1228.

[18] V.A. Sethuraman, J.W. Weidner, A.T. Haug, S. Motupally, L.V. Protsailob, Journal of the Electrochemical Society, 155 (2008) B50-B57.

[19] L. Ghassemzadeh, T.J. Peckham, T. Weissbach, X. Luo, S. Holdcroft, Journal of the American Chemical Society, 135 (2013) 15923-15932.

[20] X. Cheng, J. Zhang, Y. Tang, C. Song, J. Shen, D. Song, J. Zhang, Journal of Power Sources, 167 (2007) 25-31.

[21] H. Ito, T. Maeda, A. Nakano, H. Takenaka, International Journal of Hydrogen Energy, 36 (2011) 10527-10540.
[22] W. Tang, R. Lin, Y. Weng, J. Zhang, J. Ma, International Journal of Hydrogen Energy, 38 (2013) 10985-10991.
[23] M. Schulze, E. Gülzow, S. Schönbauer, T. Knöri, R. Reissner, Journal of Power Sources, 173 (2007) 19-27.
[24] R. Lin, E. Gülzow, M. Schulze, K.A. Friedrich, Journal of The Electrochemical Society, 158 (2011) B11.
[25] C. Yin, J. Gao, X. Wen, G. Xie, C. Yang, H. Fang, H. Tang, Energy, 113 (2016) 1071-1089.
[26] Q. Zhang, R. Lin, L. Técher, X. Cui, Energy, 115 (2016) 550-560.
[27] J. Shan, R. Lin, S. Xia, D. Liu, Q. Zhang, International Journal of Hydrogen Energy, 41 (2016) 4239-4250.
[28] M. Inaba, T. Kinumoto, M. Kiriake, R. Umebayashi, A. Tasaka, Z. Ogumi, Electrochimica Acta, 51 (2006) 5746-5753.
[29] C.E. Rogers, Permeation of Gases and Vapours in Polymers, in: J. Comyn (Ed.) Polymer Permeability, Springer Netherlands, Dordrecht , ISBN 978-94-009-4858-7, 1985, pp. 11-73.
[30] M. Schalenbach, T. Hoefner, P. Paciok, M. Carmo, W. Lueke, D. Stolten, Journal of Physical Chemistry C, (2015).
[31] S.S. Kocha, J. Deliang Yang, J.S. Yi, AIChE Journal, 52 (2006) 1916-1925.
[32] H. Zhang, J. Li, H. Tang, Y. Lin, M. Pan, International Journal of Hydrogen Energy, 39 (2014) 15989-15995.
[33] Y. Wang, N.A. Lane, C.N. Sun, F. Fan, T.A. Zawodzinski, A.P. Sokolov, Journal of Physical Chemistry B, 117 (2013) 8003-8009.
[34] M.H. Eikerling, P. Berg, Soft Matter, 7 (2011) 5976.
[35] D. Gerteisen, N. Zamel, C. Sadeler, F. Geiger, V. Ludwig, C. Hebling, International Journal of Hydrogen Energy, 37 (2012) 7736-7744.
[36] E.J. Roche, M. Pineri, R.D. †, Journal of Polymer Science Polymer Physics Edition, 20 (1982) 107–116.
[37] S.J. Paddison, Annual Review of Materials Research, 33 (2003) 289-319.
[38] J.T. Hinatsu, M. Mizuhata, H. Takenaka, J.T. Hinatsu, H. Takenaka, Journal of the Electrochemical Society, 141 (1994) 1493-1498.
[39] T.A. Zawodzinski, C. Derouin, S. Radzinski, R.J. Sherman, V.T. Smith, T.E. Springer, S. Gottesfeld, Journal of the Electrochemical Society, 140 (1993) 1041-1047.
[40] K.-D. Kreuer, Solid State Ionics, 252 (2013) 93-101.

[41] R. Hiesgen, S. Helmly, T. Morawietz, X.-Z. Yuan, H. Wang, K.A. Friedrich, Electrochimica Acta, 110 (2013) 292-305.
[42] M. Bodner, C. Hochenauer, V. Hacker, Journal of Power Sources, 295 (2015) 336-348